IEEE Access
Multidisciplinary ⋮ Rapid Review ⋮ Open Access Journal

Received 13 September 2022, accepted 22 September 2022, date of publication 26 September 2022,
date of current version 6 October 2022.

Digital Object Identifier 10.1109/ACCESS.2022.3209795

RESEARCH ARTICLE

Dynamic Electrical Models of Perovskite Solar Cells Considering Hysteresis and Charge Accumulations Effects by Using Equilibrium Optimizer

AHMED SAEED ABDELRAZEK[1], RAGAB A. EL-SEHIEMY[1], (Senior Member, IEEE), HEGAZY REZK[2], RANIA M. GHONIEM[3], POLYCARPOS FALARAS[4], AND ALAA A. ZAKY[1]

[1]Faculty of Engineering, Kafrelsheikh University, Kafr El-Sheikh 33511, Egypt
[2]Electrical Engineering Department, Faculty of Engineering, Minia University, Minia 61517, Egypt
[3]Department of Information Technology, College of Computer and Information Sciences, Princess Nourah bint Abdulrahman University, Riyadh 11671, Saudi Arabia
[4]National Center for Scientific Research "Demokritos," Institute of Nanoscience and Nanotechnology, Agia Paraskevi, Attikis, 15341 Athens, Greece

Corresponding author: Ragab A. El-Sehiemy (elsehiemy@eng.kfs.edu.eg)

This work was supported by the Princess Nourah bint Abdulrahman University Researchers Supporting Project number (PNURSP2022R138), Princess Nourah bint Abdulrahman University, Riyadh, Saudi Arabia.

ABSTRACT Perovskite solar cells (PSCs) are third-generation photovoltaic technology that has gained a lot of attention due to its technological and economic advantages. The PSCs are characterized with low cost, high absorption, long carrier diffusion length, and low fabrication temperature. To model the performance of PSCs, a new dynamic model is proposed to track the cells hysteresis by adding a variable voltage capacitor to the single, double, and triple diode models. The aim with adding the variable capacitor is to emulate the effect of charge accumulation at the interfaces of the device. Three modified models are presented based on one or more variable capacitors at single, double, and triple diode models. Where, the triple diode model with third order variable voltage capacitor model is the best among all models by 74.9% enhancement in comparison with single diode model. Also, the Equilibrium optimization algorithm (EOA) is proposed to determine the parameters of the proposed dynamic model based on the triple diode model. In comparison with the experimental data, for both forward and reverse scans, the findings showed that the suggested model accurately reflects cell performance. Added to that, the EOA finds well the optimal model parameters considering the root mean square as primary objective function. Based on the simulation results, it was proved that the proposed model gives very close results to reality.

INDEX TERMS Perovskite solar cells (PSCs), PSC hysteresis, PSCs dynamic model, equilibrium optimization algorithm.

I. INTRODUCTION

The modern life with its facilities imposes an increasing energy demand. There are two points of view to face this demand the first one is to manage the power system, the second one is to add new sources like thermopower generation [1] using new nanomaterials [2], [3] for electronic which also minimize the losses and the renewable energy sources like wind energy and solar energy and hybrid power systems [4]. The solar energy is the most widely used which attract research in many ways like improvement of the generation process via new technologies [5] to increase the generation efficiency. Another way is to improve its estimated parameters [6] to involve it in circuit design and to improve the distribution system performance under uncertainty of renewable power resources [7]

Since 2009, a considerable interest in perovskite materials has been aroused. These materials are direct band-gap

The associate editor coordinating the review of this manuscript and approving it for publication was Z. G. Zang.

semi-conductors with high absorbance, long carrier diffusion length, and high open circuit voltage, allowing them to be used in photo voltaic generation [8], [9]. Perovskite solar cells (PSCs) offer a promising path to high performance [10], [11], [12], [13], and as a result, this type of solar cell is receiving a lot of attention. Since 2009, the power conversion efficiency (PCE) of PSCs has increased from 3.8 % [14] to over 25 % [15], [12]. The J-V curve is examined by adjusting the applied voltage and recording the current density that arises from this operating voltage to better understand the electrical processes in any solar cell. So, maximum power conversion efficiencies (PCEs) of the devices can be achieved and electrical model parameters can be obtained. Hysteresis in the J-V characteristics is one of the main shor0. tcomings of PSCs, and because of this, determining the maximum power point [16] and electrical model parameters accurately are challenging. The Perovskite has also different promising applications in other fields as light emitting diodes [17], encoding [18] and near infrared emission [19], [20]. The electrical model parameters estimation for PSCs has been started from the silicon solar cells modeling examined in previous research namely single-diode model (SDM) which reflects the diffusion and recombination in the emitter quasi-neutral regions and majority zones, the double-diode model (DDM) in addition to SDM function, it reflects the recombination process in the space charge region. The three-diode model (TDM) has been recently designed and introduced to account for losses and recombination in defect zones and grain boundaries [21]. Also, there have been more sophisticated models have been introduced for multi crystalline silicon solar cells as modified DDM and modified TDM.

Many modelling issues may be solved using one of two methodologies: mathematics (analytical and numerical approaches) or computer vision techniques. In recent decades, metaheuristic algorithms have grown commonplace in a variety of fields due to higher performance and lower computational power and time requirements than deterministic algorithms [22].

Metaheuristic algorithms are often inspired by real-world phenomenon, such as mimicking physical laws or biological phenomena to find better heuristic solutions to optimization issues. The two main types of metaheuristic algorithms are swam-based approaches and evolutionary procedures.

Evolutionary approaches and smart swarm techniques are the two main types of methodologies influenced by nature. The evolutionary algorithm (EA) was inspired by nature's biological evolution phase. In comparison to the traditional optimization technique, it is a more robust and widely applicable global optimization technique.

Some of the popular algorithms in the EA class used to solve engineering problems are Genetic Programming (GP) [23], Genetic Algorithm [24], Evolutionary Programming EP) [25], Evolution Strategy (ES) [26] and Differential Evolution [27]. Furthermore, the usage of ES and EP in scientific research and practical problems is growing in popularity. Swarm Intelligence [28] is a social intelligence or collective that models the decentralization of biological groups in nature or the collective behavior of self-organizing systems artificially. Biological groupings in nature that have collective behaviors and knowledge to accomplish a goal are typically the source of inspiration for this class of algorithms. Because SI algorithms are accessible to the appliance, they are often more advantageous than evolutionary algorithms; nonetheless, evolutionary algorithms have fewer operators to supervise. Furthermore, the SI algorithm is better than EA in recording and utilizing past data. Established and recent algorithms in this class to solve engineering problems are: Particle Swarm Optimization (PSO) [6], Bat-inspired Algorithm [29], Coyote optimization algorithm [30], Bald Eagle Search Optimizer [31], Wasp Swarm Optimization [32], Grey Wolf Optimization [33], Moth Flame Optimization [34], slime mould algorithm [35], Artificial Bee Colony [36], Harris Hawk Optimizer [37], and Ant Colony Optimization [38].

There are also some metaheuristic algorithms simulate mostly physical phenomena by employing mathematical rules or approaches to solve engineering problems such as: Charged System Search [39], Gravitational Search Algorithm [40], Sine Cosine Algorithm [41], Simulated Annealing [42], Tabu Search [43], and Teaching-Learning-Based Optimization [44].

A novel optimization technique Equilibrium Optimizer (EO) [45] is inspired by control volume mass balance models that is utilized to anticipate both dynamic and equilibrium states in this work. In EO, each particle (solution) acts as a search agent, and its concentration determines how effective it is (position). The search agents' concentration is updated at random with relation to the best-so-far solutions, namely equilibrium candidates, to arrive at the equilibrium state. The best of our knowledge is that the TDM has the closest characteristic to the experimental one [46], [47], however it has not been able to simulate hysteresis in PSCs yet. The hysteresis and stability issues are the main reasons that PSCs still not commercialized till now but a lot of studies based in new techniques like interface engineering succeeded to fix these problems [48], [49], [50], [51].

It is worth to mention that PSCs production costs are very low in the case of perovskite-based devices compared to silicon-based devices since 1-watt costs almost 10 to 20 cents; in contrast, 1 watt in silicon-based cells costs almost 75 cents, while 1 watt produced by thermoelectric generator costs 70 cents as presented in [52] and [53]. Previous studies proved that the hysteresis phenomena in PSCs are one of the main problems of these devices [10], [11], [12], [13], [14], [15], [16], [17], [18], [19], [20] and there is necessity to model it in order to solve this problem. This work proposes a novel variable voltage capacitor (VVC) based TDM (VVCTDM) which has succeeded to simulate and emulate the PSCs hysteresis that fits well with the experimental characteristics. This variable voltage capacitor is suggested to reflect the effect of charge accumulation at the device interfaces at its

different operation dynamics. The main contribution of this paper can be summarized as:

- Proposed three variable capacitor-based PSCs models by using variable voltage capacitor (VCC) which accounts the cumulative charge effect.
- Considering the forward and reverse scan rates of the J-V measurements in the model to emulate the PSCs device hysteresis.
- Solving the SDM, DDM and TDM with proposed linear, second order and third order VVC.
- Proposing a modified VCC-based triple diode model for PSCs simulation.
- Developing the equilibrium optimization algorithm to solve the proposed model.

This work is organized as follows: Section II presents the experimental work; PSCs modeling is presented in section III; section IV presents the Equilibrium optimization algorithm. The simulation and experimental results are presented in section V and, respectively. The conclusions are presented in section VI.

II. EXPERIMENTAL WORK

The Perovskite solar cell is fabricated in this work as follows; Fluorine-doped tin oxide (FTO) conductive glasses sonicated via sonication bath each 15 minutes in the order of Hellmanex, 2-propanol, and acetone for cleaning. Electron Transporting Layer (ETL) which is also called titania layer was spin coated over the cleaned FTO glasses after 15 minutes UV ozone treatment. The detailed steps to fabricate the device are shown in Fig. 1.

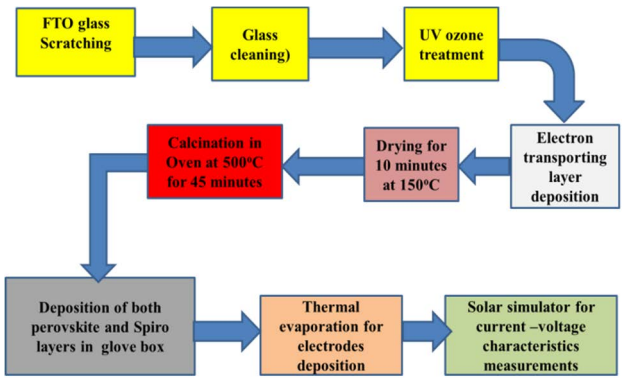

FIGURE 1. Schematic diagram for perovskite solar cell fabrication procedures.

It was made up of four layers over fluorine tine oxide (FTO) conductive glasses as presented in Fig. 2 and was constructed as follows:

Electron Transport Layer (layer 1): This layer was made by depositing a TiO2 compact layer on FTO conductive glasses (Sigma Aldrich, 7 Ohm·cm^{-2}). FTO conductive glass was etched in solution of a 6m HCl/H_2O with Zn powder, then cleaned in a sonication path with Hellmanex, 2-propanol, and acetone. Each stage took 15 minutes. At last, a 15-minute UV ozone treatment is used to remove any leftover dust. A TiO_2 compact layer has been deposited over the cleaned FTO conductive glasses using a spin coating process at 2000 r.p.m. for 1 minute using an ethanolic solution of titanium (IV) isopropoxide containing a tiny amount of HCl, after FTO cleaning. For 10 minutes, the films were dried at 150 °C over a hot plate after the spin coating procedure, then for 45 minutes it exposed to 500 °C (5°C·min-1 temperature ramp rate).

Absorber layer (Perovskite layer) (layer 2): The perovskite active absorber layer MAPbI3 was deposited on the titania compact layer in the glovebox using a perovskite solution of Lead acetate trihydrate in a 3:1 molar ratio and 40 wt percent Methylammonium iodide mixed in anhydrous DMF and spun for 45 seconds at 2000 r.p.m. Finally, hypophosphorous acid (50 percent w/w, aquatic solution) has been added to the solution, resulting in an HPA: $PbAc_2$ molar ratio of 1:4. After drying for 10 minutes at ambient temperature, the films were annealed at 100 °C for 5 minutes. Fig. 3.a depicts the reverse and forward scans of the device J-V curves, whereas Fig.3.b depicts the absorbance of the perovskite layer deposited on a TiO_2 compact layer substrate.

Hole transporting layer (Spiro-MeOTAD) (layer 3): The Spiro-MeOTAD was employed as a hole transporting layer and was made from chlorobenzene (7wt%) with additives of bis (trifluoromethanesulfonyl) imide lithium salt (dissolved in acetonitrile) and 4-tert-butylpyridine (deposited by spin coating at 4000 r.p.m for 10s). Silver Electrodes (layer 3): At last, using a thermal evaporator (10^{-6}Torr and $\sim$1Å·s^{-1} rate), six silver electrodes with a thickness of 100 nm were deposited outside the glovebox. The experimental records are added as supplementary information to this manuscript.

III. PROPOSED PSCS MODELS

PSCs are made up of three primary layers: an electron transport layer (TiO_2), the perovskite absorber (active layer), and the hole transporter layer (Spiro-OMeTAD), as depicted in Fig. 2.b. Photons are absorbed at the perovskite layer and forms electron and hole pairs, which pass through the electron transport layer and the hole transport layer, respectively. Charges accumulate in the perovskite/Electron transport layer, perovskite/hole transport layer interfaces, and the perovskite layer itself if it is nonhomogeneous because the

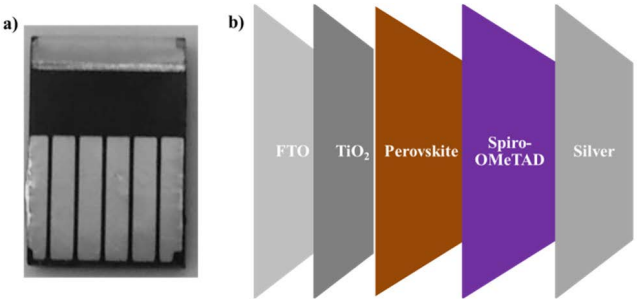

FIGURE 2. The perovskite solar cell architecture a) Laboratory fabricated device b) Device schematic diagram.

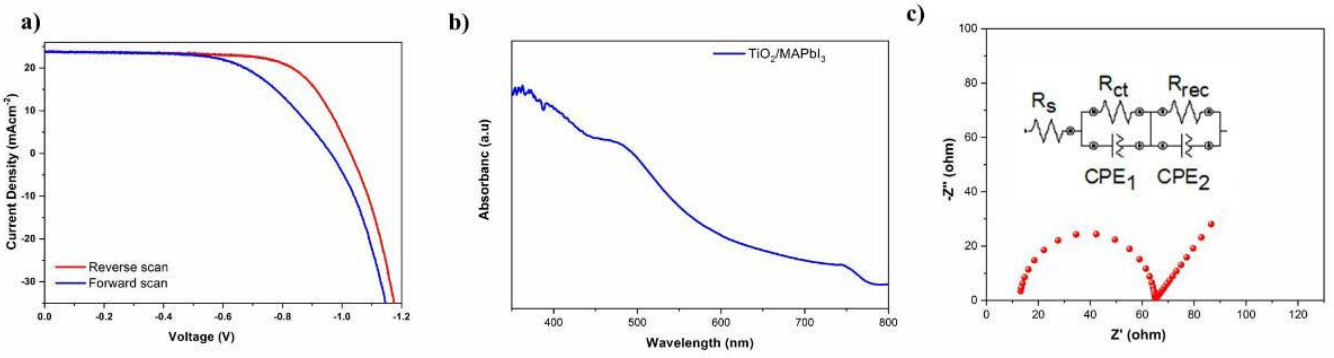

FIGURE 3. Perovskite solar cell characteristics a) Device J-V curves (reverse and forward scans) b) Absorbance of perovskite ($MAPbI_3$) upon TiO_2 substrate c) Device impedance.

rate of generation of electron and hole pairs is faster than the rate of transfer through the electron and hole transporting layers. Additional R-C circuits indicate charge accumulation at interfaces, as shown in Fig. 4.a. Hysteresis in PSCs is mainly caused by charge accumulation at the corresponding interfaces also depends on the scan rate during measuring the J-V curves. As a result, charge accumulation (C_{eq}) and scan rate (last term in Eq. 1) considers the hysteresis effect.in PSC modelling. Because the shunt resistances R_{p1}, R_{p2}, and R_{p3} are all quite large, we can ignore their effect as shown in Fig. 5. The charge accumulation at perovskite/Electron transport layer interface is represented by C_3 while, the charge accumulation at perovskite layer itself if it is nonhomogeneous is represented by C_2 and the charge accumulation at the perovskite /Hole transport layer interface is modeled by C_1. From Fig. 4b it is evident that the three capacitances are connected in series. Figure 5 represents the VVCTDM, which is the modification to general formulation of the TDM to account the charge accumulations effect which represented by Eq 1 as:

$$\begin{aligned} I_s = I_{ph} &- k_1.I_{s1}\left[\exp\left(\frac{q\,(V_t + R_s.I_s)}{(m_1)\cdot k\cdot T}\right) - 1\right] \\ &- k_2.I_{s2}\left[\exp\left(\frac{q\,(V_t + R_s.I_s)}{(m_2)\cdot k\cdot T}\right) - 1\right] \\ &- k_3.I_{s3}\left[\exp\left(\frac{q\,(V_t + R_s.I_s)}{(m_3)\cdot k\cdot T}\right) - 1\right] \\ &- \frac{V_t + R_s.I_s}{R_{sh}} - C_{eq}\frac{d(V + R_s.I_s)}{dt} \end{aligned} \tag{1}$$

where j_{ph} is the photo-generated current (A), I_{s1} is the reverse saturation current of diode 1 (A), I_{s2} is the reverse saturation current of diode 2 (A), I_{s3} is the reverse saturation current of diode 3 (A), m_1 is the ideality factor for diode 1, m_2 is the ideality factor for diode 2, m_3 is the ideality factor for diode 3, R_s is the series resistance (Ω), R_{sh} is the shunt resistance (Ω), V is the output voltage of the cell (V), K is the Boltzmann's constant ($1.38065e^{-23}$ J/K) and T is the cell temperature (K). k_1, k_2 *and* k_3 are three binary parameters to model various PV models and these values are arranged as: for SDM: $k_1 = 1$, $k_2 = k_3 = 0$, for DDM: $k_1 = k_2 = 1$ *and* $k_3 = 0$ and for TDM: $k_1 = k_2 = k_3 = 1$

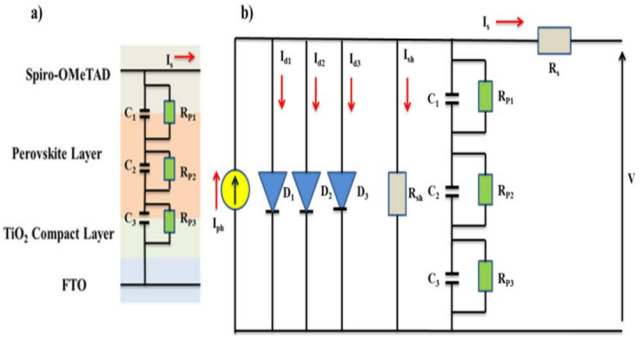

FIGURE 4. a) Perovskite solar cells equivalent circuit with capacitors that representing the charge accumulation at device interfaces, b) General triple diode model including charge accumulations effect for PSCs.

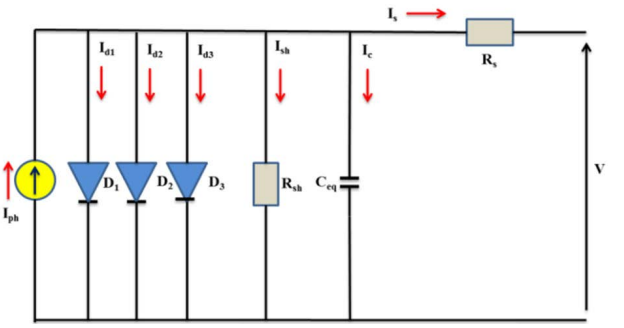

FIGURE 5. Simplified triple diode model including charge accumulations effect for PSCs.

The resulting capacitors are highly affected by the different layer bias; it is suggested that the resultant capacitances are variable dependent and might be expressed in terms of applied potential and current density by linear, second order and third order equations, as shown below in Eq. (2).

$$C_{eq} = a + b(V + R_S.I_s) \tag{2.a}$$

$$C_{eq} = a + b(V + R_S.I_s) + c(V + R_S.I_s)^2 \tag{2.b}$$

$$C_{eq} = a + b(V + R_S.I_s) + c(V + R_S.I_s)^2 + d(V + R_S.I_s)^3 \tag{2.c}$$

where a, b, c and d are positive parameters depending on the chosen model. Eq. 3 gives the fitness function of the suggested model as:

$$f\ (V_t, j_t, y) = I_s = I_{ph} - k_1.I_{s1}\left[\exp\left(\frac{q\,(V_t + R_s.I_s)}{(m_1)\cdot k\cdot T}\right) - 1\right] - k_2.I_{s2}\left[\exp\left(\frac{q\,(V_t + R_s.I_s)}{(m_2)\cdot k\cdot T}\right) - 1\right] - k_3.I_{s3}\left[\exp\left(\frac{q\,(V_t + R_s.I_s)}{(m_3)\cdot k\cdot T}\right) - 1\right] - \frac{V_t + R_s.I_s}{R_{sh}} - C_{eq}\frac{d(V + R_s.I_s)}{dt} - I_{meas} \quad (3)$$

where f is the error function, I_{meas} represents the measured current of the tested solar cell.

IV. EQUILIBRIUM OPTIMIZATION ALGORITHM

This study introduces a novel optimization technique called EO, inspired by control volume mass balance models used to predict both dynamic and equilibrium states. Each particle (solution) functions as a search agent in EO, with its concentration (position). To arrive at the equilibrium state, the search agents update their concentration at random regarding the best-so-far solutions, namely the optimal result of equilibrium candidates. The main steps performed are as follow:

$$X_i = LI + Rand(UI - LI) \quad (4)$$

where X_i represents the individual particles' i^{th} generation, Ul and Ll represent the search space upper and lower limits and Rand represents a uniform distributed random vector between 0 and 1.

A. EQUILIBRIUM POOL

Following initialization, the four particles with the minimum error are chosen to create the equilibrium pool, which is updated after each iteration.

$$X_{eqp} = \{X_{eqp1}, X_{eqp2}, X_{eqp3}, X_{eqp4}, X_{eqpave}\} \quad (5)$$

where X_{eqp1}, X_{eqp2}, X_{eqp3} and X_{eqp4} represent the four best individual, X_{eqp} represents the equilibrium pool and X_{eqpave} represent the four individual average particles:

$$X_{eqpave} = (X_{eqp1} + X_{eqp2} + X_{eqp3} + X_{eqp4})/4 \quad (6)$$

B. EXPONENTIAL TERM

By varying the exponential term E, EO balances the algorithm's exploitation and exploration. The following is a description of E's mathematical formula:

$$E = a_1.\text{sign}\,(R - 0.5)\,.\left(e^{-\lambda p} - 1\right) \quad (7)$$

where a1=2, λ and R represent uniform random vectors of values from 0 to 1, p represents a coefficient that varies nonlinearly as in Eqs. (8) as:

$$p = (1 - \frac{\text{iter}}{\text{iter}_{max}})^{(a_2.\frac{\text{iter}}{\text{iter}_{max}})} \quad (8)$$

where iter represents the present iteration number, iter_{max} represents the maximum iterations number and $a_2 = 1$.

C. GENERATION RATE

The generation rate G is a significant component influencing EO's performance and shows EO's ability to use data in the optimization process. The following is a description of the mathematical model:

$$G = GCP.(X_{eqp} - \lambda X_i) \quad (9)$$

where GCP is a control vector which is calculated from:

$$GCP = \begin{cases} 0.5r_2, & r_3 \geq GP \\ 0, & r_3 < GP \end{cases} \quad (10)$$

X_{eqp} is a particle selected randomly from the equilibrium pool, X_i represents the present particle, r_2 and r_3 are uniformly distributed random numbers from 0 to 1 and GP represent a constant equals 0.5.

In summary, the following equation can be used to generate candidate particles using EO:

$$X = X_{eq} + (X - X_{eq})\,.E + \frac{G}{\lambda v}(1 - E) \quad (11)$$

where v can be regarded a unit volume.

By modulating the contribution of the second and third terms through E, EO balances the algorithm's exploitation and exploration, where the second and third terms help exploration and exploitation respectively.

V. RESULTS AND DISCUSSION

The experimental J-V characteristic curves of the PSCs are shown in Fig. 3.d. The most different feature between the silicon solar cells and the PSCs other than the efficiency is the hysteresis between forward and backward scan. Table 1 summarizes the main features of the proposed PSC for forward and backward scans. The proposed models in this study were solved by the equilibrium algorithm in order to find the best fit curves and device parameters with the experimental results. The main idea is to generate a theoretical curve based on the proposed models and compare it with the experimental ones and to find the best one fits under the lowest deviation. As a result, the optimal; parameters of the device are obtained. A brief numerical study of the proposed PSCs as has been performed to find the best equivalent circuit suitable. The equilibrium algorithm has been operated on three models namely SDM, DDM and TDM then notice the deviation from the experimental results, after that check how far the VVCTDM modification is suitable. The results revealed that the TDM is the best one to model the PSCs performance with hysteresis effect.

TABLE 1. Photovoltaic parameters for the tested device.

Scan direction	J_{sc} (mA cm^{-2})	V_{oc} (V)	FF	PCE (%)	Hysteresis index
Reverse scan	23.78	1.03	0.70	16.97	20 %
Forward scan	23.79	0.96	0.60	13.62	

where, Voc: open-circuit voltage, JSC: short-circuit current density, FF: fill factor, PCE: power conversion efficiency.

TABLE 2. Optimal parameters of the dynamic TDM and three modified models for hysteresis in PCSs.

Model	I_{ph}(A)	I_{s1}(μA)	m_1	R_{sh}(Ω)	R_s(Ω)	I_{s2}(A)	m_2	I_{s3}(A)	m_3	A	b	c	d
TDM	0.02360	3.42E-05	5.337	441.390	0.0001	1.03E-13	6.49597	1.00E-13	4.8735	-	-	-	-
MTDM1	0.02369	6.21E-05	8.516	368.896	0.3993	1.09E-13	3.74462	7.34E-06	4.491	0.0308	1.00E-12	-	-
MTDM2	0.02350	2.41E-07	3.43	699.966	0.57695	0.000119	7	1.02E-13	6.3377	0.0259	0.0103	1.01E-12	-
MTDM3	0.02387	1.00E-13	6.586	271.065	0.64438	5.15E-06	4.27675	1.00E-13	5.6688	0.0203	1.05E-12	0.01715	2.61E-06

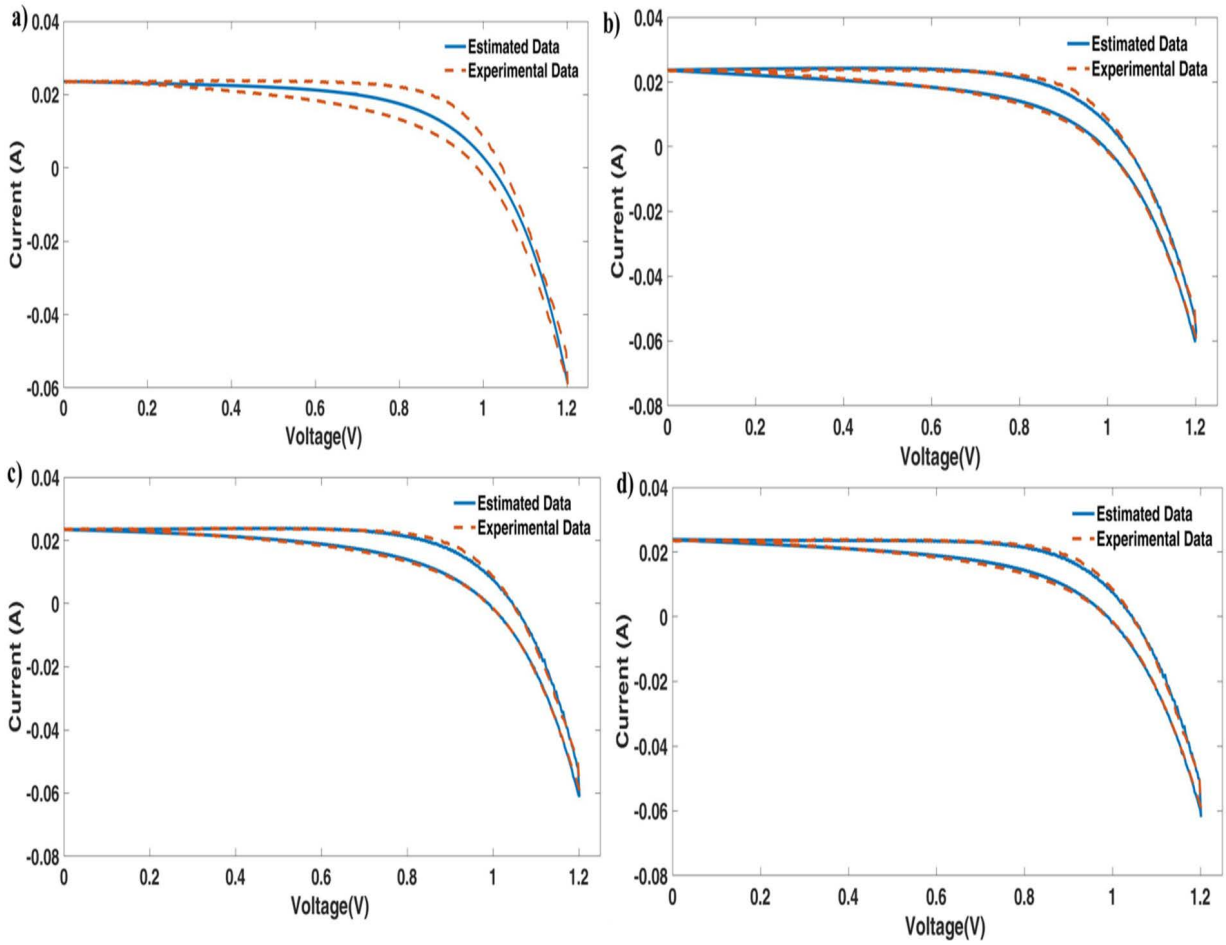

FIGURE 6. The experimental and estimated current- voltage curves: a) TDM without capacitor, b) MTDM1 including the capacitor according to Eq.2a, c) MTDM2 including the capacitor according to Eq.2b, d) MTDM3 including the capacitor according to Eq.2c.

TABLE 3. Statistical analysis of the TDM and its modifications parameters using EOA.

Model	Best RMSE	Worst RMSE	Average RMSE	Standard Deviation
TDM	0.003193444488	0.0032069909	0.003195538	2.815043e-06
MTDM1	0.001126184019	0.002019942599	0.001202342	0.0001214705
MTDM2	0.001011725135	0.002000945411	0.001174705	0.0001488815
MTDM3	0.0009630068154	0.001295694903	0.001137535	0.0001002782

Experimental data and the estimated circuit of the traditional SDM which was not able to simulate the hysteresis with RMSE of 0.00383 while, Fig. 8b shows the J-V curve for the experimental data and the estimated circuit of the SDM after adding a linear VVC (Eq. 2a) which improve the RMSE to 0.00319 by 16.7% over the SDM, even the hysteresis has not been simulated well enough. The improvement in the results is because of the consideration of charge accumulation at the layers interfaces which has been modeled by the capacitor. After modifying the VVC to second order equa-

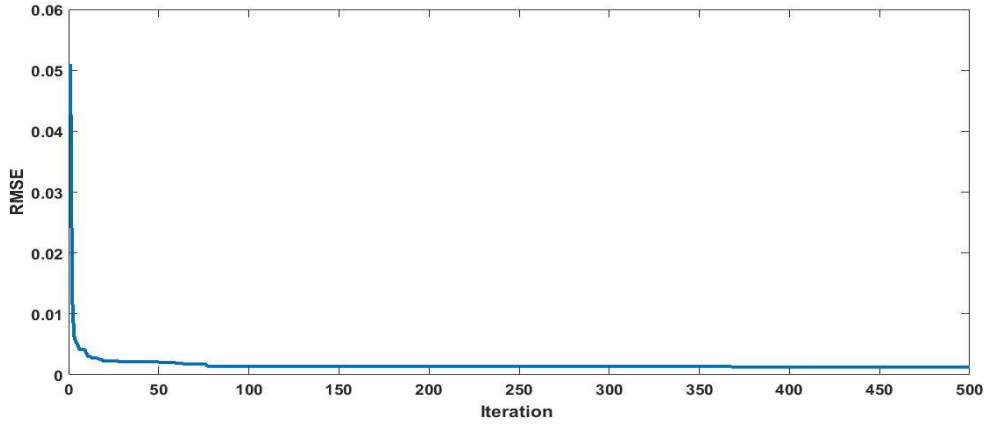

FIGURE 7. The convergence curve for the MTDM3 case.

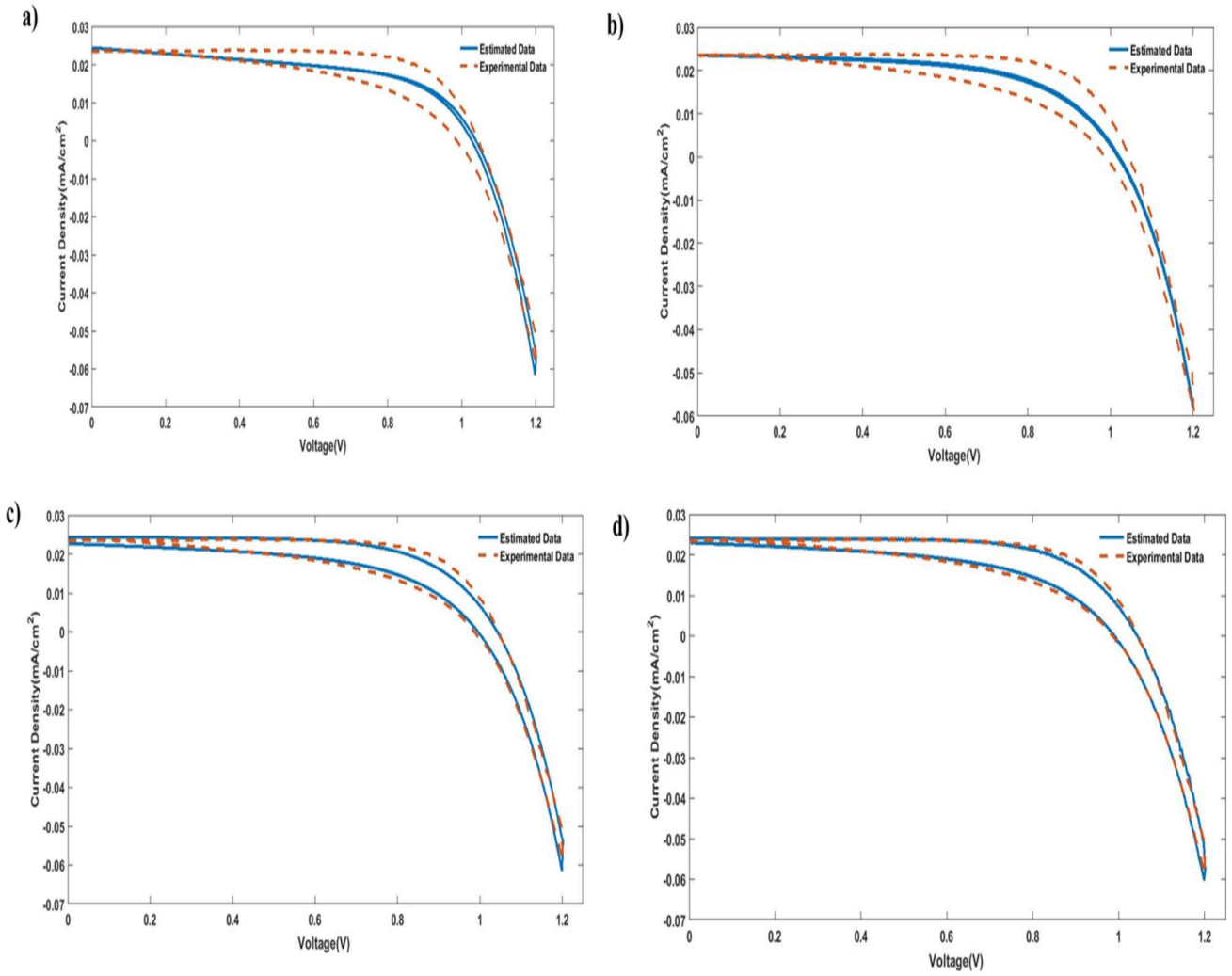

FIGURE 8. a) SDM without capacitor; b) MSDM1 including the capacitor according to Eq.2a; c) MSDM2 including the capacitor according to Eq.2b; d) MSDM3 including the capacitor according to Eq.2c.

tion (Eq.2b) the calculations show much better results in the hysteresis representation (Fig. 8c) and the RMSE improved to 0.00128 with 60% over the linear VVC because of representing more charge accumulation places and more nonlin-

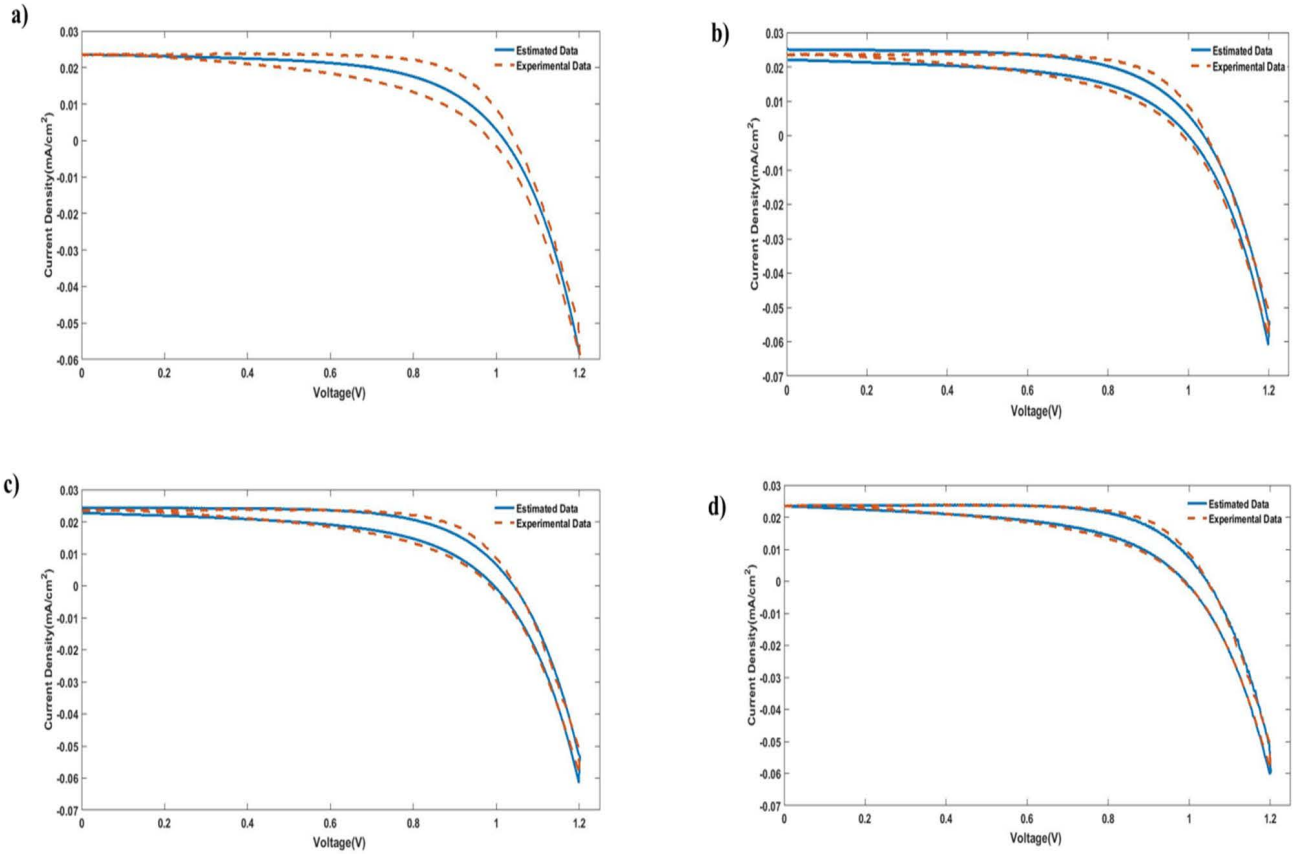

FIGURE 9. a) DDM without capacitor; b) MDDM1 including the capacitor according to Eq.2a; c) MDDM2 including the capacitor according to Eq.2b; d) MDDM3 including the capacitor according to Eq.2c.

TABLE 4. The estimated parameters resulted by EO on PV SDM.

Model	I_{ph}(A)	I_s(A)	m	R_{sh}(Ω)	R_s(Ω)	a	B	c	d
SDM	0.0246	7.070977e-08	2.9999999	128.99622	0.96582095	-	-	-	-
MSDM1	0.0235772	3.508581e-05	5.3530006	461.82003	0.0001	0.0017873075	0.0002532994	-	-
MSDM2	0.0235489	2.396259e-05	5.0991766	424.92461	0.13704617	0.0099497249	0.009999940	0.0056582468	-
MSDM3	0.023577	1.115613e-05	4.6450760	373.72581	0.45742456	0.0094737179	0.0099939128	0.0099981361	0.003541223

TABLE 5. The statistical analysis of the SDM and its modifications parameters resulted from the optimization process.

Model	Best RMSE	Worst RMSE	Average RMSE	Standard Deviation
SDM	0.003833305176	0.004754068851	0.003962145	0.0001995136
MSDM1	0.003193455697	0.003654136357	0.003202867	6.512172e-05
MSDM2	0.001276267541	0.00160443098	0.001306272	6.680943e-05
MSDM3	0.001069308649	0.001304874081	0.001221244	6.485038e-05

earity. The best of the SDM modifications is the third order VVC according to eq. 2c (Figure 8d) with 0.00107 RMSE which is 16.4% better than the Second order VVC because of including all the places of the charge accumulation including the three capacitors and the higher nonlinearity, the convergence curve of this case is shown in Figure 9 Table 4 represents the estimated parameters resulted from application of EO on PV SDM and the proposed modifications to simulate the hysteresis. While Table 5 represents the statistical analysis of the SDM and its modifications parameters resulted from the optimization process and it is clear the best closeness has been resulted from the third order variable voltage capacitor.

TABLE 6. The estimated parameters resulted from application of EO on PV DDM and the proposed modifications.

Model	I_{ph}(A)	I_{s1}(A)	m_1	R_{sh}(Ω)	R_s(Ω)	I_{s2}(A)	m_2	a	b	c	d
DDM	0.023592	2.2213e-13	4.99968	449.67581	0.0001	3.44912e-5	5.3426773	-	-	-	-
MDDM1	0.02359	5.70752e-8	8.35931	441.13811	1.00035e-5	3.34278e-5	5.32281	0.01	0.00987912	-	-
MDDM2	0.023547	2.72493e-5	5.1769453	452.4803	0.11741244	1.0064e-13	5.0970135	0.01	0.01	0.00551121	-
MDDM3	0.023561	3.0179e-06	4.1509893	428.51305	0.5383256	4.8819e-5	6.9102139	0.0148026	1.0001e-12	0.0201511	5.343e-06

TABLE 7. The statistical analysis of the DDM and its modifications parameters resulted from the optimization.

Model	Best RMSE	Worst RMSE	Average RMSE	Standard Deviation
DDM	0.003193438991	0.003211708093	0.003196233	4.717803e-06
MDDM1	0.001604291486	0.002237049252	0.001624127	8.954808e-05
MDDM2	0.001277312817	0.002472648059	0.001332427	0.0001753869
MDDM3	0.001006668827	0.001308248821	0.001165836	.636623e-05

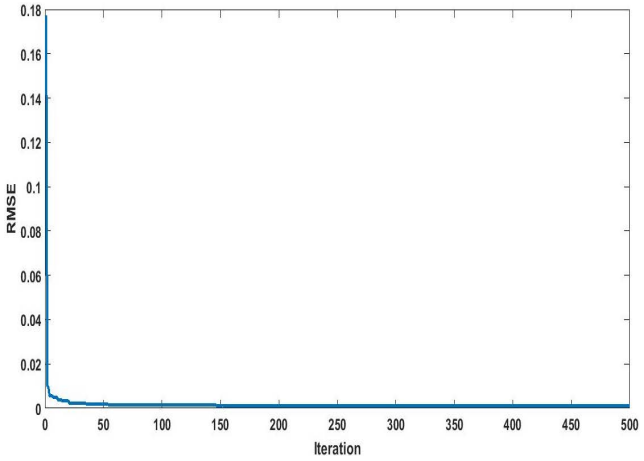

FIGURE 10. The convergence curve for the MSDM3 case.

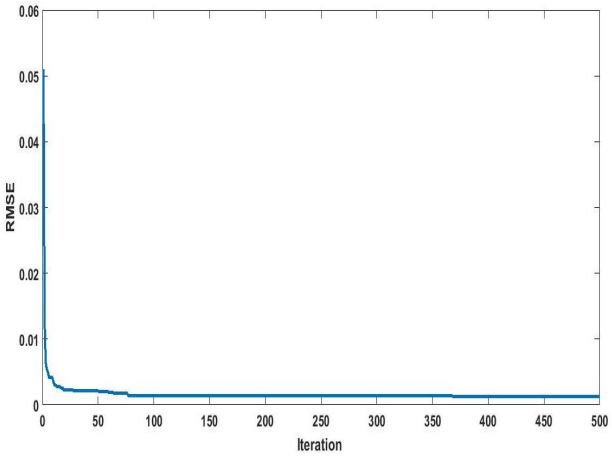

FIGURE 11. The convergence curve for the MDDM3 case.

Figure 10a shows the J-V curve for the experimental data and the estimated circuit of the traditional DDM which was not able to simulate the hysteresis with RMSE of 0.00319. Figure 10b shows the J-V curve for the experimental data and the estimated circuit of the DDM after adding a linear VVC which improved the RMSE to 0.00160 by 50% over the DDM, also the hysteresis has been simulated well enough. After modifying the VVC to second order equation the calculations show better results in the hysteresis representation (Figure 10c) and the RMSE improved to 0.00128 with 20% over the linear VVC. The best of the DDM modifications is the third order VVC (Figure 10d) with 0.00101 RMSE which is 21.1% better than the Second order VVC and the convergence curve of the third order VVC is presented in Figure 11. Table 6 represents the estimated parameters resulted from application of EO on PV DDM and the proposed modifications to simulate the hysteresis. While, Table 7 represents the statistical analysis of the DDM and its modifications parameters resulted from the optimization process and it is clear the best closeness has been resulted from the third order variable voltage capacitor. The overall results show that, for SDM the best is the one with third order VVC by 72% over the traditional SDM. Also, the third order VVC is the best of the DDM over the traditional one by 68.3% and for the TDM the third order VVC is the best over the traditional one by 69.9%. Finally, the third order VVC of the TDM is the closest to the experimental which 74.9% closer than the SDM.

VI. CONCLUSION

New proposed perovskite solar cell dynamic electric models called single-, double- and triple-diode models have been studied in this study. For accurate modeling the hysteresis characteristics, variable linear, second order and third order voltage capacitors are emulated in the proposed models to represent charge accumulation at device interfaces on the device performance. The proposed models were solved using the Equilibrium Optimization algorithm, in all models the ones that have third order capacitor are the best where in single diode model 72% enhancement over the traditional model (without capacitor) is achieved, 68.3% in the double diode model and 69.9% in the triple diode model. The results were

quite close to the experimental ones in the triple diode model including third order voltage capacitors case and successfully simulated the device performance in both steady state and dynamic modes and very close to the experimental results by 74.9% more that the single diode model. The findings confirmed the validity of the suggested model for simulating the dynamic performance of the perovskite solar cells.

APPENDIX A: SIMULATIONS RESULTS OF SINGLE- AND DOUBLE- DIODE MODELS

See Figures 8–11 and Tables 4–7.

ACKNOWLEDGMENT

The authors sincerely acknowledge the support from the Princess Nourah bint Abdulrahman University Researchers Supporting Project number (PNURSP2022R138), Princess Nourah bint Abdulrahman University, Riyadh, Saudi Arabia.

REFERENCES

[1] M. M. El-Banna, A. H. Phillips, and A. S. A. Bayoumi, "Ferromagnetic silicene superlattice based thermoelectric flexible renewable energy generator device," *IEEE Access*, vol. 9, pp. 103564–103572, 2021, doi: 10.1109/access.2021.3098042.

[2] M. M. El-Banna, A. H. Phillips, and A. S. A. Bayoumi, "Spin-valley thermoelectric characteristics of ferromagnetic silicene superlattice," *Ain Shams Eng. J.*, vol. 12, no. 2, pp. 2193–2203, Jun. 2021, doi: 10.1016/j.asej.2021.01.002.

[3] A. S. Abdelrazek, M. M. El-banna, and A. H. Phillips, "Photon-spin coherent manipulation of piezotronic nanodevice," *Micro Nano Lett.*, vol. 11, no. 12, pp. 876–880, Dec. 2016, doi: 10.1049/mnl.2016.0264.

[4] A. M. Shaheen, E. E. Elattar, R. A. El-Sehiemy, and A. M. Elsayed, "An improved sunflower optimization algorithm-based Monte Carlo simulation for efficiency improvement of radial distribution systems considering wind power uncertainty," *IEEE Access*, vol. 9, pp. 2332–2344, 2021, doi: 10.1109/ACCESS.2020.3047671.

[5] Z. Shi, J. Guo, Y. Chen, Q. Li, Y. Pan, H. Zhang, Y. Xia, and W. Huang, "Lead-free organic-inorganic hybrid perovskites for photovoltaic applications: Recent advances and perspectives," *Adv. Mater.*, vol. 29, no. 16, Apr. 2017, Art. no. 1605005, doi: 10.1002/adma.201605005.

[6] A. S. Bayoumi, R. A. El-Sehiemy, K. Mahmoud, M. Lehtonen, and M. M. F. Darwish, "Assessment of an improved three-diode against modified two-diode patterns of MCS solar cells associated with soft parameter estimation paradigms," *Appl. Sci.*, vol. 11, no. 3, p. 1055, Jan. 2021.

[7] E. S. Ali, R. A. El-Sehiemy, A. A. Abou El-Ela, K. Mahmoud, M. Lehtonen, and M. M. F. Darwish, "An effective bi-stage method for renewable energy sources integration into unbalanced distribution systems considering uncertainty," *Processes*, vol. 9, no. 3, p. 471, Mar. 2021, doi: 10.3390/pr9030471.

[8] Y. Zhao and K. Zhu, "Organic–inorganic hybrid lead halide perovskites for optoelectronic and electronic applications," *Chem. Soc. Rev.*, vol. 45, no. 3, pp. 655–689, 2016, doi: 10.1039/c4cs00458b.

[9] X. Peng, J. Yuan, S. Shen, M. Gao, A. S. R. Chesman, H. Yin, J. Cheng, Q. Zhang, and D. Angmo, "Perovskite and organic solar cells fabricated by inkjet printing: Progress and prospects," *Adv. Funct. Mater.*, vol. 27, no. 41, Nov. 2017, Art. no. 1703704, doi: 10.1002/adfm.201703704.

[10] C. Dai, W. Chen, Y. Zhu, and X. Zhang, "Seeker optimization algorithm for optimal reactive power dispatch," *IEEE Trans. Power Syst.*, vol. 24, no. 3, pp. 1218–1231, Aug. 2009, doi: 10.1109/TPWRS.2009.2021226.

[11] Q. Zhuang, H. Wang, C. Zhang, C. Gong, H. Li, J. Chen, and Z. Zang, "Ion diffusion-induced double layer doping toward stable and efficient perovskite solar cells," *Nano Res.*, vol. 15, no. 6, pp. 5114–5122, Jun. 2022, doi: 10.1007/s12274-022-4135-7.

[12] S. Li, J. Liu, S. Liu, D. Zhang, C. Liu, D. Li, J. Qi, Y. Hu, A. Mei, and H. Han, "Yttrium-doped Sn_3O_4 two-dimensional electron transport material for perovskite solar cells with efficiency over 23%," *EcoMat*, vol. 4, no. 4, p. e12202, Jul. 2022, doi: 10.1002/eom2.12202.

[13] Y. Zhu, L. Shu, Q. Zhang, Y. Zhu, S. Poddar, C. Wang, Z. He, and Z. Fan, "Moth eye-inspired highly efficient, robust, and neutral-colored semitransparent perovskite solar cells for building-integrated photovoltaics," *EcoMat*, vol. 3, no. 4, p. e12117, Aug. 2021, doi: 10.1002/eom2.12117.

[14] A. Kojima, K. Teshima, Y. Shirai, and T. Miyasaka, "Organometal halide perovskites as visible-light sensitizers for photovoltaic cells," *J. Amer. Chem. Soc.*, vol. 131, no. 17, pp. 6050–6051, May 2009, doi: 10.1021/ja809598r.

[15] N. J. Jeon, H. Na, E. H. Jung, T.-Y. Yang, Y. G. Lee, G. Kim, H.-W. Shin, S. Il Seok, J. Lee, and J. Seo, "A fluorene-terminated hole-transporting material for highly efficient and stable perovskite solar cells," *Nature Energy*, vol. 3, no. 8, pp. 682–689, Aug. 2018, doi: 10.1038/s41560-018-0200-6.

[16] H. J. Snaith, A. Abate, J. M. Ball, G. E. Eperon, T. Leijtens, N. K. Noel, S. D. Stranks, J. T.-W. Wang, K. Wojciechowski, and W. Zhang, "Anomalous hysteresis in perovskite solar cells," *J. Phys. Chem. Lett.*, vol. 5, no. 9, pp. 1511–1515, Mar. 2014, doi: 10.1021/jz500113x.

[17] K. Shen, J. Wang, Y. Shen, Y. Li, M. Guo, Z. Su, L. Lu, X. Cai, L. Chen, F. Song, X. Gao, J. Tang, and N. Ueno, "Unraveling the role of crystallization dynamics on luminescence characteristics of perovskite light-emitting diodes," *Laser Photon. Rev.*, vol. 15, no. 7, Jul. 2021, Art. no. 2100023, doi: 10.1002/lpor.202100023.

[18] Y. Zhong, B. Tang, M. Fei, Q. Jie, J. Tan, Q. Wang, S. Liang, J. Du, L. Zhang, H. Dong, and W. Xie, "All-photonic miniature perovskite encoder with a terahertz bandwidth," *Laser Photon. Rev.*, vol. 14, no. 4, Apr. 2020, Art. no. 1900398, doi: 10.1002/lpor.201900398.

[19] R. Wu, P. Han, D. Zheng, J. Zhang, S. Yang, Y. Zhao, X. Miao, and K. Han, "All-inorganic rare-Earth-based double perovskite nanocrystals with near-infrared emission," *Laser Photon. Rev.*, vol. 15, no. 11, Nov. 2021, Art. no. 2100218, doi: 10.1002/lpor.202100218.

[20] T. Li, T. Xiang, M. Wang, W. Zhang, J. Shi, M. Shao, T. Xu, M. Ahmadi, X. Wu, Z. Gao, L. Xu, and P. Chen, "Unraveling the energy landscape and energy funneling modulated by hole transport layer for highly efficient perovskite LEDs," *Laser Photon. Rev.*, vol. 15, no. 4, Apr. 2021, Art. no. 2000495, doi: 10.1002/lpor.202000495.

[21] A. S. Bayoumi, R. A. El-Sehiemy, K. Mahmoud, M. Lehtonen, and M. M. F. Darwish, "Assessment of an improved three-diode against modified two-diode patterns of MCS solar cells associated with soft parameter estimation paradigms," *Appl. Sci.*, vol. 11, no. 3, pp. 1–20, Feb. 2021, doi: 10.3390/app11031055.

[22] H. Faris, A. M. Al-Zoubi, A. A. Heidari, I. Aljarah, M. Mafarja, M. A. Hassonah, and H. Fujita, "An intelligent system for spam detection and identification of the most relevant features based on evolutionary random weight networks," *Inf. Fusion*, vol. 48, pp. 67–83, Aug. 2019, doi: 10.1016/j.inffus.2018.08.002.

[23] J. R. Koza and J. P. Rice, "Automatic programming of robots using genetic programming," in *Proc. AAAI*, vol. 92, pp. 194–207, 1992.

[24] L. B. Booker, D. E. Goldberg, and J. H. Holland, "Classifier systems and genetic algorithms," *Artif. Intell.*, vol. 40, nos. 1–3, pp. 235–282, Sep. 1989.

[25] X. Yao, Y. Liu, and G. Lin, "Evolutionary programming made faster," *IEEE Trans. Evol. Comput.*, vol. 3, no. 2, pp. 82–102, Jul. 1999.

[26] N. Hansen, S. D. Müller, and P. Koumoutsakos, "Reducing the time complexity of the derandomized evolution strategy with covariance matrix adaptation (CMA-ES)," *Evol. Comput.*, vol. 11, no. 1, pp. 1–18, Mar. 2003.

[27] R. Storn and K. Price, "Differential evolution—A simple and efficient heuristic for global optimization over continuous spaces," *J. Global Optim.*, vol. 11, no. 4, pp. 341–359, Dec. 1997.

[28] G. Beni and J. Wang, "Swarm intelligence in cellular robotic systems," in *Robots and Biological Systems: Towards a New Bionics?* Berlin, Germany: Springer, 1993, pp. 703–712.

[29] T. Niknam, S. Sharifinia, and R. Azizipanah-Abarghooee, "A new enhanced bat-inspired algorithm for finding linear supply function equilibrium of GENCOs in the competitive electricity market," *Energy Convers. Manag.*, vol. 76, pp. 1015–1028, Dec. 2013, doi: 10.1016/j.enconman.2013.08.012.

[30] A. Abaza, R. A. El Sehiemy, and A. S. A. Bayoumi, "Optimal parameter estimation of solid oxide fuel cell model using coyote optimization algorithm," in *Recent Advances in Engineering Mathematics and Physics*. Cham, Switzerland: Springer, 2020, pp. 135–149.

[31] A. Abaza, R. A. El Sehiemy, A. El-Fergany, and A. S. A. Bayoumi, "Optimal parameter estimation of solid oxide fuel cells model using bald eagle search optimizer," *Int. J. Energy Res.*, vol. 46, no. 10, pp. 13657–13669, Aug. 2022.
[32] P. C. Pinto, T. A. Runkler, and J. M. C. Sousa, "Wasp swarm algorithm for dynamic MAX-SAT problems," in *Proc. Int. Conf. Adapt. Natural Comput. Algorithms*, 2007, pp. 350–357.
[33] A. Habibollahzade, I. Fakhari, S. Mohsenian, H. Aberoumand, and R. A. Taylor, "Multi-objective grey wolf optimization of solar chimneys based on an improved model incorporating a wind turbine power curve," *Energy Convers. Manage.*, vol. 239, Jul. 2021, Art. no. 114231, doi: 10.1016/j.enconman.2021.114231.
[34] A. A. Elsakaan, R. A. El-Sehiemy, S. S. Kaddah, and M. I. Elsaid, "An enhanced moth-flame optimizer for solving non-smooth economic dispatch problems with emissions," *Energy*, vol. 157, pp. 1063–1078, Aug. 2018, doi: 10.1016/j.energy.2018.06.088.
[35] R. Djekidel, B. Bentouati, M. S. Javaid, H. R. E. H. Bouchekara, A. S. Bayoumi, and R. A. El-Sehiemy, "Mitigating the effects of magnetic coupling between HV transmission line and metallic pipeline using slime mould algorithm," *J. Magn. Magn. Mater.*, vol. 529, Jul. 2021, Art. no. 167865, doi: 10.1016/j.jmmm.2021.167865.
[36] X. Yuan, P. Wang, Y. Yuan, Y. Huang, and X. Zhang, "A new quantum inspired chaotic artificial bee colony algorithm for optimal power flow problem," *Energy Convers. Manage.*, vol. 100, pp. 1–9, Aug. 2015, doi: 10.1016/j.enconman.2015.04.051.
[37] Y. Liu, G. Chong, A. A. Heidari, H. Chen, G. Liang, X. Ye, Z. Cai, and M. Wang, "Horizontal and vertical crossover of Harris hawk optimizer with Nelder–Mead simplex for parameter estimation of photovoltaic models," *Energy Convers. Manage.*, vol. 223, Nov. 2020, Art. no. 113211, doi: 10.1016/j.enconman.2020.113211.
[38] M. Kefayat, A. Lashkar Ara, and S. A. N. Niaki, "A hybrid of ant colony optimization and artificial bee colony algorithm for probabilistic optimal placement and sizing of distributed energy resources," *Energy Convers. Manage.*, vol. 92, pp. 149–161, Mar. 2015, doi: 10.1016/j.enconman.2014.12.037.
[39] A. Kaveh and S. Talatahari, "A novel heuristic optimization method: Charged system search," *Acta Mechanica*, vol. 213, nos. 3–4, pp. 267–289, 2010.
[40] O. Özkaraca and A. Keçebaş, "Performance analysis and optimization for maximum exergy efficiency of a geothermal power plant using gravitational search algorithm," *Energy Convers. Manage.*, vol. 185, pp. 155–168, Apr. 2019, doi: 10.1016/j.enconman.2019.01.100.
[41] J. Wang, W. Yang, P. Du, and T. Niu, "A novel hybrid forecasting system of wind speed based on a newly developed multi-objective sine cosine algorithm," *Energy Convers. Manage.*, vol. 163, pp. 134–150, May 2018, doi: 10.1016/j.enconman.2018.02.012.
[42] J. A. Alfaro-Ayala, O. A. López-Núñez, F. I. Gómez-Castro, J. J. Ramírez-Minguela, A. R. Uribe-Ramírez, J. M. Belman-Flores, and S. Cano-Andrade, "Optimization of a solar collector with evacuated tubes using the simulated annealing and computational fluid dynamics," *Energy Convers. Manage.*, vol. 166, pp. 343–355, Jun. 2018, doi: 10.1016/j.enconman.2018.04.039.
[43] S. Pothiya, I. Ngamroo, and W. Kongprawechnon, "Application of multiple Tabu search algorithm to solve dynamic economic dispatch considering generator constraints," *Energy Convers. Manage.*, vol. 49, no. 4, pp. 506–516, Apr. 2008, doi: 10.1016/j.enconman.2007.08.012.
[44] M. Abdel-Basset, R. Mohamed, R. K. Chakrabortty, K. Sallam, and M. J. Ryan, "An efficient teaching-learning-based optimization algorithm for parameters identification of photovoltaic models: Analysis and validations," *Energy Convers. Manage.*, vol. 227, Jan. 2021, Art. no. 113614, doi: 10.1016/j.enconman.2020.113614.
[45] A. Faramarzi, M. Heidarinejad, B. Stephens, and S. Mirjalili, "Equilibrium optimizer: A novel optimization algorithm," *Knowl.-Based Syst.*, vol. 191, Mar. 2020, Art. no. 105190, doi: 10.1016/j.knosys.2019.105190.
[46] R. Chenouard and R. A. El-Sehiemy, "An interval branch and bound global optimization algorithm for parameter estimation of three photovoltaic models," *Energy Convers. Manage.*, vol. 205, Feb. 2020, Art. no. 112400, doi: 10.1016/j.enconman.2019.112400.
[47] M. A. El-Dabah, R. A. El-Sehiemy, M. Becherif, and M. A. Ebrahim, "Parameter estimation of triple diode photovoltaic model using an artificial ecosystem-based optimizer," *Int. Trans. Electr. Energy Syst.*, vol. 31, Jul. 2021, Art. no. e13043, doi: 10.1002/2050-7038.13043.
[48] A. Zaky, M. Ibrahim, and H. Rezk, "Energy efficiency improvement of water pumping system using synchronous reluctance motor fed by perovskite solar cells," *Int. J. Energy Res.*, vol. 44, no. 14, pp. 11629–11642, 2020, doi: 10.1002/er.5788.
[49] A. A. Zaky, R. A. E. Sehiemy, Y. I. Rashwan, M. A. Elhossieni, K. Gkini, A. Kladas, and P. Falaras, "Optimal performance emulation of PSCs using the elephant herd algorithm associated with experimental validation," *ECS J. Solid State Sci. Technol.*, vol. 8, no. 12, pp. Q249–Q255, 2019, doi: 10.1149/2.0271912jss.
[50] A. A. Zaky, A. Fathy, H. Rezk, K. Gkini, P. Falaras, and A. Abaza, "A modified triple-diode model parameters identification for perovskite solar cells via nature-inspired search optimization algorithms," *Sustainability*, vol. 13, no. 23, p. 12969, Nov. 2021, doi: 10.3390/su132312969.
[51] T. Zhou, M. Wang, Z. Zang, and L. Fang, "Stable dynamics performance and high efficiency of ABX_3-type super-alkali perovskites first obtained by introducing H_5O_2 cation," *Adv. Energy Mater.*, vol. 9, no. 29, 2019, Art. no. 1900664, doi: 10.1002/aenm.201900664.
[52] Z. Song, C. Mcelvany, A. Phillips, and I. Çelik, "A technoeconomic analysis of perovskite solar module manufacturing with low-cost materials and techniques," *Energy Environ. Sci.*, vol. 10, no. 6, pp. 1297–1305, 2017, doi: 10.1039/C7EE00757D.
[53] Z. Ouyang and D. Li, "Design of segmented high-performance thermoelectric generators with cost in consideration," *Appl. Energy*, vol. 221, pp. 112–121, Jul. 2018, doi: 10.1016/j.apenergy.2018.03.106.

AHMED SAEED ABDELRAZEK was born in Cairo, Egypt, in 1983. He received the B.Sc. degree in electronics and communication engineering and the M.Sc. and Ph.D. degrees from Ain Shams University, Egypt, in 2005, 2013, and 2016, respectively. He is currently an Associate Professor with the Engineering Physics and Mathematics Department, Faculty of Engineering, Kafrelsheikh University, Egypt. His research interests include spin transport properties in nanostructures and its applications, optimization PV and its applications, and renewable energy.

RAGAB A. EL-SEHIEMY (Senior Member, IEEE) was born in Menoufia, Egypt, in 1973. He received the B.Sc. degree in electrical engineering and the M.Sc. and Ph.D. degrees from Menoufia University, Egypt, in 1996, 2005, and 2008, respectively. He is currently a Full Professor with the Electrical Engineering Department, Faculty of Engineering, Kafrelsheikh University, Egypt. He was a receipt of Prof. Mahmoud Khalifia Award in power system engineering from the Academy of Research and Technology, Egypt, in 2016. He was also a receipt of El-Shorouk Academy Award in computer and information applications in industry from the Academy of Research and Technology, in 2020. He is one of the top 2% effective researchers among the worlds, in 2021. He has published more than 190 articles in international journals and conferences. His research interests include power systems operation, planning and control, smart grid, renewable energy, and AI and its application to power systems.

HEGAZY REZK received the B.Eng. and M.Eng. degrees in electrical engineering from Minia University, Egypt, in 2001 and 2006, respectively, and the Ph.D. degree from the Moscow Power Engineering Institute, Moscow. He was a Postdoctoral Research Fellow with the Moscow State University of Mechanical Engineering, Russia, for six months. He was a Visiting Researcher at Kyushu University, Japan, for one year. He is currently an Associate Professor with the Electrical Engineering Department, Collage of Engineering at Wadi Addwaser, Prince Sattam University, Saudi Arabia. His current research interests include renewable energy, smart grid, hybrid systems, power electronics, optimization, and artificial intelligence.

RANIA M. GHONIEM received the Ph.D. degree in integrating artificial intelligence techniques in medical diagnosis from Mansoura University, Egypt. She is currently working with the Department of Information Technology, College of Computer and Information Sciences, Princess Nourah Bint Abdulrahman University, Riyadh, Saudi Arabia. Her research interests include computer-aided diagnostic systems, medical image and sound processing, natural language processing, deep learning, and meta-heuristic optimization methods.

POLYCARPOS FALARAS was born in Karditsa, Greece, in 1960. He received the degree in physics from the Aristotle University of Thessaloniki, Greece, the D.E.A. degree (Hons.) in electrochemistry from the University Pierre et Marie Curie, Paris VI, France, in 1983, and the Ph.D. degree (Hons.) in chemistry, in 1986. He joined the Physique des Liquides et Electrochimie Laboratory, CNRS, University Pierre et Marie Curie. In 1989, he entered the National Center for Scientific Research ''Demokritos,'' Athens, Greece, where he is currently working as the Research Director, leading a group of 16 people. He disposes strong expertise in research management and he has been the Director of the NCSR Demokritos, Institute of Physical Chemistry, from 2007 to 2012. He has published more than 290 articles in international refereed journals, more than 16.000 citations, and H-index 6. He holds seven patents. He is participated, including coordination of several EU and national projects. He is currently working on nanomaterials and nanotechnology-driven processes for solar energy conversion to electricity (third generation solar cells: dye-sensitized, quantum dot, perovskite) and environmental protection (photocatalytic materials and reactors for water cleaning, CO_2 capture/conversion). He is an Editor of *Applied Catalysis B: Environmental*, a member of the editorial board in seven international journals, and a reviewer of more than 100 international refereed journals. He is teaching physical chemistry at Hellenic Open University. He has supervised the work of 15 postdoctoral and 13 Ph.D. students and serves regularly as an Expert Evaluator and a Reviewer of EU programs (Marie Curie and Energy). For his innovative work in photoinduces processes, he has been awarded by international (Prince Sultan International Prize for Water—PSIPW, Alternative Water Resources Prize), and national (Theodoros Aretaios Award, Academy of Athens) organizations.

ALAA A. ZAKY received the B.Sc. degree in electrical power and machines engineering from Kafrelsheikh University, Egypt, in 2007, the M.Sc. degree in electrical power and machines engineering from Mansoura University, Egypt, in 2015, and the Ph.D. degree in electrical engineering from the School of Electrical and Computer Engineering, National Technical University of Athens, in 2021. In 2008, he became a Teaching Staff with the Electrical Engineering Department, Kafrelsheikh University, where he has been an Assistant Professor with the Department of Electrical Engineering, since 2021. His current research interests include renewable energy, solar energy technologies, third generation solar cells, optimization, power system operation, and control. He received several times the Kafrelsheikh University Award for his international scientific publications.